Journal of Solid State Electrochemistry (2018) 22:3515–3525
https://doi.org/10.1007/s10008-018-4041-9

ORIGINAL PAPER

Electrochemical sensor using graphene/Fe_3O_4 nanosheets functionalized with garlic extract for the detection of lead ion

Bin He[1] · Xian-feng Shen[1] · Jing Nie[1] · Xiao-li Wang[1] · Fang-mei Liu[2] · Wei Yin[1] · Chang-jun Hou[3] · Dan-qun Huo[3] · Huan-bao Fa[1]

Received: 21 January 2018 / Revised: 5 July 2018 / Accepted: 7 July 2018 / Published online: 2 August 2018

Abstract

Based on the modulated electronic properties of Fe_3O_4-graphene (Fe_3O_4/GN composite) as well as the outstanding complexation between Pb^{2+} and natural substances garlic extract (GE), a novel electrochemical sensor for the determination of Pb^{2+} in wastewater was prepared by immobilization of Fe_3O_4/GN composite integrated with GE onto the surface of glassy carbon electrode (GCE). Fe_3O_4/GN composite was employed as an electrochemical active probe for enhancing electrical response by facilitating charge transfer while GE was used to improve the selectivity and sensitivity of the proposed sensor to Pb^{2+} assay. The electrochemical sensing performance toward Pb^{2+} was appraised by cyclic voltammetry (CV), electrochemical impedance spectroscopy (EIS), and square wave voltammetry (SWV). Under the optimized condition, the sensor exhibited two dynamic linear ranges (LDR) including 0.001 to 0.5 nM and 0.5 to 1000 nM with excellent low detection limit (LOD) of 0.0123 pM ($S/N = 3$) and quantification limit (LOQ) of 0.41 pM ($S/N = 10$). Meanwhile, it displayed remarkable stability, reproducibility (RSD of 3.61%, $n = 3$), and selectivity toward the assay for the 100-fold higher concentration of other heavy metal ions. Furthermore, the novel sensor has been successfully employed to detect Pb^{2+} from real water samples with satisfactory results.

Keywords Garlic extract · Lead(II) · Fe_3O_4/GN · Electrochemical sensor

Introduction

Garlic (*Allium sativum* L.) is a worldwide cultivated Alliaceae species and of economic benefits in food and medicine. In the previous research, garlic is effective in treating lead intoxication for workers who are exposed to environmental lead. In general, garlic and its derivatives have been gradually recommended as a promising agent for lead treatment because of the negative effect of the chelating agents that can deplete the body of essential metals resulting in secondary injury for health [1]. The positive effects of garlic on human health are ascribed to the presence of bioactive substances such as organosulfur compounds [2–5], flavonoids, and vitamins [6]. The organosulfur compounds mainly include diallyl trisulfide, diallyl tetrasulfide, s-allylcysteine, vinyldithiines, allylpropyl disulfide, ajonens ((E) - and (Z)-4, 5, 9–trithiadodeca-1, 6, 11–triene-9- oxides), and allicin [5, 7–9]. The components are likely to work synergistically to provide the largest range of garlic's health benefits. To the best of our knowledge, Fatima and Ahmad [10] have utilized the antioxidant enzymes of garlic as biomarkers of heavy metals for detecting the heavy metals in wastewater. Cheng et al. [11] and Zhou et al. [12] have fabricated electrochemical sensors for determining Pb^{2+} based on L-cysteine. However, garlic has not been explored in the field of electrochemical sensor to detect the presence of Pb^{2+} in wastewater, which is expected to attract particular attention for the detection of Pb^{2+} by virtue of their simple operation modes, rapid

Electronic supplementary material The online version of this article (https://doi.org/10.1007/s10008-018-4041-9) contains supplementary material, which is available to authorized users.

✉ Wei Yin
yinweicqu@163.com

✉ Huan-bao Fa
huanbaofa@cqu.edu.cn

[1] National-Municipal Joint Engineering Laboratory for Chemical Process Intensification and Reaction, College of Chemistry and Chemical Engineering, Chongqing University, Chongqing 400044, People's Republic of China

[2] FuJian Key Laboratory for Green Production of Copper and Comprehensive Utilization of Associated Resources, Zijin Copper Co., Ltd, Shanghang county, Longyan City, Fujian province 364204, People's Republic of China

[3] Key Laboratory of Biorheology Science and Technology, Ministry of Education, College of Bioengineering, Chongqing University, Chongqing 400044, People's Republic of China

response, high sensitivity, and selectivity [13]. Hence, in this study, garlic extract (GE), as a natural product, may provide a sensitive electrochemical interface in the field of electrochemical sensor and pre-concentrate Pb^{2+} to produce stable complexes for the recognition of Pb^{2+} in wastewater.

Nonetheless, the preponderances of GE heavily rely on the supporting materials which are in possession of high specific surface area, superior electronic conductivity, and easy functionalization. Based on these criterions, graphene is an ideal supporting material [14]. Graphene (GN) has a unique nanostructure and interesting properties (such as large surface, excellent conductive property, prominent thermal stability) [15], which results in widespread potential applications, like supercapacitors [16] or serving as absorbent of heavy metal ions [17]. However, it has been widely reported that the graphene-metal oxide nanomaterials have better functionalization and performance in their applications than graphene or metal oxide nanomaterials solely [14, 18], resulting from inheriting the advantages of two component materials [19–21]. Therefore, it is an interesting and appealing method that Fe_3O_4 nanoparticles are grown and anchored on GN sheets as supporting material for the electrode of electrochemical sensor, combining with the fascinating merits of Fe_3O_4 NPs and GN and exhibiting a better electrochemical performance compared with the native phase [21–27]. Suryawanshi et al. [28] have successfully prepared a Fe_3O_4 hierarchically perforated graphene nanosheets composite with enhanced electronic conductivity. Zhou et al. [29] have synthesized a well-organized flexible interleaved GNS/Fe_3O_4 composite through in situ reduction of iron hydroxide between graphene nanosheets (GNS), behaving superior electrochemical performance. Furthermore, the incorporation of Fe_3O_4 NPs onto graphene sheets tackled the aggregation of Fe_3O_4 nanoparticles and preserved the electrochemically active surface of Fe_3O_4 NPs [30]. Thus, the Fe_3O_4/GN composite is a remarkable electrode material for electrochemical sensor. Based on this background, in this study, Fe_3O_4/GN composite as an electrochemical active probe could enhance the electrical response by facilitating charge transfer.

The main purpose of this investigation was to develop a simple, sensitive, selective, and inexpensive electrochemical method for the determination of Pb^{2+} in wastewater. In the current work, a simple and novel electrochemical sensor with high sensitivity and selectivity has been on the spotlight for Pb^{2+} determination in wastewater by using Fe_3O_4/GN/GE-modified glassy carbon electrode (GCE). The electrode preparation is described in Scheme 1. The GE and Fe_3O_4/GN composite are chosen as the modifier for GE is an economical nature product and Fe_3O_4/GN composite is environmentally friendly, respectively. To the best of our knowledge, this is the first work describing and integrating the unique features of both Fe_3O_4/GN composite and GE through fabricating a sensor to exploit their synergy for the electrochemical detection of Pb^{2+}. It was found that the proposed sensor is allowed to select optimal conditions for the detection of Pb^{2+}, showing satisfactory linearity, detection limit, sensitivity, selectivity, and high reproducibility and stability. Relative to the reported methods [31–34], the established method has superior electrochemical properties. Furthermore, the experiment results of determination Pb^{2+} in real samples by the developed sensor are also acceptable. Thus, not only does Fe_3O_4/GN/GE sensor represent a new electrochemical platform for designing environment-friendly sensors but also could meet the needs of practical analysis.

Experiment

Chemicals and apparatus

Aged garlic was purchased from a local market (Chongqing, China). Graphene oxide (GO) was provided by Sigma-Aldrich. All other chemicals, such as $FeSO_4 \cdot 7H_2O$, NaOH, and $N_2H_4 \cdot H_2O$, were of analytical grade purity and purchased from Tianjin Chemical Technology Co., Ltd. (China) without further purification. Unless otherwise stated, the supporting electrolyte is a 0.1 mol/L acetate buffer solution (ABS, pH 5.50). The double-distilled water was used for all solutions.

The morphologies of the as-prepared samples were acquired on a JSM-7500F (Hitachi Co., Ltd., Japan) scanning electron microscope and Tecnai G20 transmission electron microscope (FEI Company, USA). The crystallographic information was recorded by a XRD-6000 classical powder diffractometer with Cu kα radiation ($\lambda = 0.154$ nm). The function groups of the samples were gathered by a Nicolet 550 FTIR Spectrometer (Shimadzu Scientific Instruments) from 400 to 4000 cm^{-1} at room temperature.

GC–MS analysis of the garlic extract (GE) was performed with a 6890N gas chromatograph (Agilent, American) system equipped with a fused silica capillary Agilent Technology HP-5 ms (5% phenyl methyl siloxane) column (30 m × 0.25 mm i.d., film thickness 0.1 μm) and a 5975C plus mass spectrometer (Agilent, American). For GC–MS detection, 1 μL sample was injected for analysis. In the GC system, injector and detection temperature were set at 280 and 290 °C, respectively. The initial temperature was kept at 40 °C for 2 min and ramped to 130 °C with a rate of 8 °C/min, then increased to 290 °C (10 min) at a rate of 10 °C/min. Carrier gas was helium with flow rate of 1 mL/min. A 70-eV EI mode with an ionic source temperature of 230 °C was used in the MS system. The standard mass spectra of organosulfur compounds were provided by literature data and the software of the GC-MS system

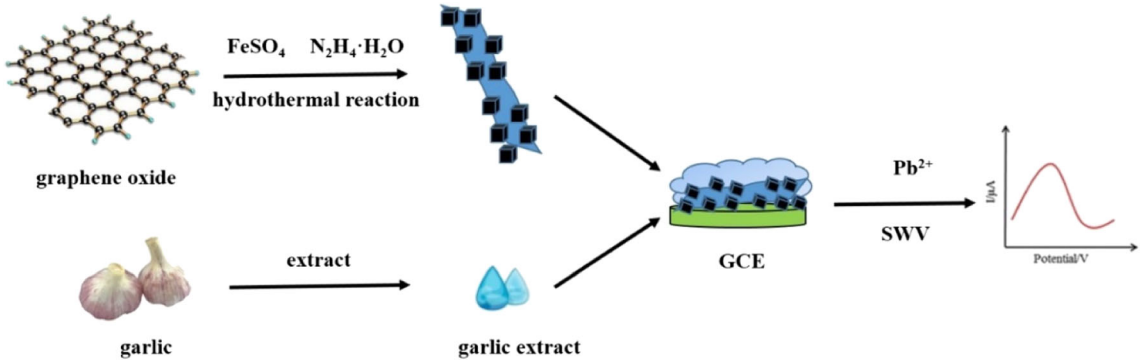

Scheme 1 The preparation process of Fe3O4/GN/GE electrochemical detection of Pb2+.

(National Institute of Standards and Technology (NIST 05. LIB) libraries date).

A CHI660E electrochemical workstation (ChenHua Instrument Co., Shanghai, China) was used to perform the electrochemical experiments, including cyclic voltammetry (CV) and square wave voltammetry (SWV). Different modified glassy carbon electrodes (Fe_3O_4/GCE, Fe_3O_4/GN/GCE, Fe_3O_4/GN/GE/GCE) or a bare glassy carbon electrode (GCE, 3 mm diameter) were used as the working electrode, with an Ag/AgCl/KCl (3 mol/L KCl saturated with AgCl) and platinum wire serving as the reference and counter electrodes, respectively.

Synthesis of Fe_3O_4 and Fe_3O_4/GN

The Fe_3O_4/GN nanocomposites were synthesized by a solvethermal process with Fe_3O_4 nanoparticles attached to reduced graphene oxide (GN) sheets, which combine the controllable growth of Fe_3O_4 NPs and the reduction of GO in one single step. It was slightly modified from the method as reported by Wang et al. [35]. For preparing Fe_3O_4/GN, 20 mL of $FeSO_4 \cdot 7H_2O$ solution (a concentration of ~ 69.5 mg/mL) and 5 mL of NaOH solution (a concentration of ~ 80 mg/mL) were slowly added into the prepared 30-mL GO water suspension (a concentration of ~ 2.67 mg/mL) in order with vigorous stirring. The mixture was stirred at room temperature for 1 h. Then, 20 mL $N_2H_4 \cdot H_2O$ was injected into the solution apace and then the mixture was loaded into a 100-mL Teflon lined stainless steel autoclave for hydrothermal reaction at 180 °C for 8 h. The Fe_3O_4/GN separated by magnetic force from solution was washed with deionized water several times and then dried at 60 °C for 8 h.

For comparison, the same synthetic procedures were carried out in the preparation of Fe_3O_4 NPs but without adding GO, as the reference.

Extraction of GE

The garlic was peeled, cleaned, and dried at room temperature, followed by chopping. A 10-g chopped edible portion was kept at 50 °C for 2 h, then mixed for 1 h after the addition of 70 mL ethanol solution (anhydrous ethanol/deionized water = 7/1, *V*/*V*) at 30 °C for leaching repeatedly. After that, the mixture was filtrated and centrifugated to remove the insoluble substance. Next, the ethanol solution was evaporated from the supernate to obtain the garlic extract (GE). The GE stored at 4 °C until subsequent experiments.

Fabrication of the electrochemical sensor

The GCE ($\Phi = 3$ mm) was polished by 1.0, 0.3, and 0.05 μm alumina slurry, along with successive washing with anhydrous ethanol and deionized water, then dried through nitrogen blowing. One milligram of the synthesized Fe_3O_4/GN was dispersed in 1 mL deionized water with ultra-sonication for 2 h to acquire a homogenous suspension. Then, another 1 h of ultra-sonication was kept after 50 μL of GE mixing until a homogenously dispersed solution (Fe_3O_4/GN/GE). Afterwards, 5 μL of the resulting homogenous suspension was drop-casted onto the surface of a polished GCE and dried at room temperature. A Fe_3O_4-modified GCE sensor (Fe_3O_4/GCE) and Fe_3O_4/GN-modified GCE sensor (Fe_3O_4/GN/GCE) were also fabricated using similar procedures for comparison studies.

Electrochemical measurements

For CV experiments, 5.0 mmol/L $K_3[Fe(CN)_6]$ with 0.1 mol/L KCl standard solutions were used for evaluating electrochemical sensor performance with a scan rate of 50 mV/s from − 0.2 to + 0.7 V. Electrochemical impedance spectroscopy (EIS) measurements were performed in 5.0 mmol/L $K_3[Fe(CN)_6]$/$K_4[Fe(CN)_6]$ solution to determinate the charge transfer resistance of the modified electrodes over a frequency range of 0.1 Hz~100 kHz with amplitude of 10 mV. SWV measurements were taken in 0.1 mol/L ABS containing different concentrations of Pb^{2+} solutions (pH 5.50) in the absence of dissolved oxygen.

Results and discussion

Physicochemical characterization

GC–MS analysis of GE

The components of the garlic extract (GE) were analyzed by GC–MS. Figure 1 is a representative total ion current chromatogram of GE and Table 1 summarizes the identified compounds. Table 1 also provides the identified structure of chemical compounds and GC retention time. The garlic extract included mainly ethyl acetate, 3-methyl-butanal, 1,1-diethoxy-ethan homopolymer, 1,3-dithiane, allyl methyl disulphide, diallyl disulphide, 3-vinyl-1,2-dithiacyclohex-4-ene, 3-vinyl-1,2-dithiacyclohex-5-ene, and diallyl trisulfide, which consisted with the previous researches [4, 5].

SEM and TEM

The morphologies of as-prepared Fe_3O_4 NPs, Fe_3O_4/GN composite, and Fe_3O_4/GN/GE composite determined by SEM and TEM were shown in Fig. 2. Figure 2a, b is the SEM and TEM images of the Fe_3O_4 NPs, respectively. It can be found in the images that the Fe_3O_4 NPs consisted of cube-shaped structures of NPs with the edge length of 50–150 nm and spherical structures of NPs with the diameter of ~ 50 nm. Figure 2c, d provides the micrographs of Fe_3O_4/GN composite. It is clearly observed from SEM image that Fe_3O_4 NPs with hybrid structure were densely and uniformly anchored over the crumpled surface of GN. Meanwhile, the presence of GN did not alter the mixture cubic and spherical morphology of Fe_3O_4 NPs, but effectively decreased their particles after the composite formation. The TEM image in Fig. 2d further confirmed the present clearer structural information of the Fe_3O_4/GN sample. Valuably, the synergistic effect between the Fe_3O_4 and GN in the formation retains the unique structure and prevents the agglomeration of Fe_3O_4 NPs. In addition, the interaction between Fe_3O_4 NPs and GN makes possible Fe_3O_4 NPs strongly anchored on the surface of GN even after a long-time ultra-sonication and does not need additional molecular linker to bridge the Fe_3O_4 NPs and GN. It is noted that the GN provides large areas. Thereby, we can believe that the Fe_3O_4/GN composite can facilitate the electron transfer and remain the active surface areas to further boost the electrochemical performance of Fe_3O_4/GN electrodes benefiting from the unique structure [36]. The SEM image of Fe_3O_4/GN/GE composite shown in Fig. 2e presents an obvious change in comparison to Fe_3O_4/GN composite, which has been decorated with a GE layer on the surface of Fe_3O_4/GN composite. All of these results jointly attest the successful preparation of Fe_3O_4/GN/GE composite, which could be utilized as a remarkable biosensing platform for Pb^{2+} determination.

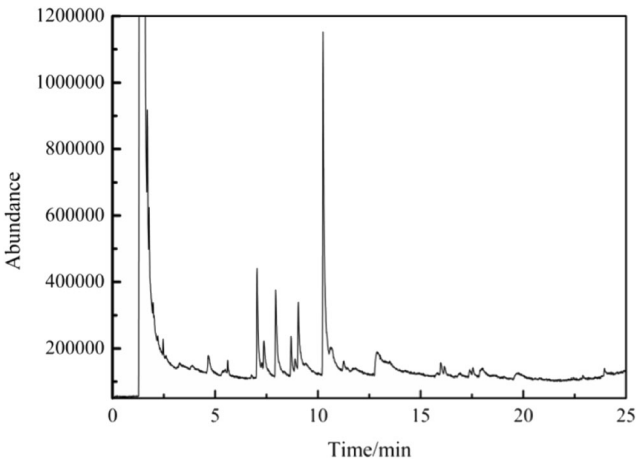

Fig. 1 Total ion current chromatogram of garlic organic components extracted by ethanol

XRD and FTIR

Figure 3a has studied the crystal phase and structure information of the prepared Fe_3O_4 NPs, Fe_3O_4/GN, and Fe_3O_4/GN/GE nanocomposite by XRD measurement. The diffraction peaks at $2\theta \approx 30.19°$, 35.62°, 43.39°, 57.01°, and 62.79° can be indexed to (2 2 0), (3 1 1), (4 0 0), (5 1 1), and (4 4 0) reflection planes of Fe_3O_4, which guaranteed the cubic structure of as-synthesized Fe_3O_4 nanostructure (JCPDS No. 01-082-1533) [15, 37]. The structure of Fe_3O_4 in Fe_3O_4/GN and Fe_3O_4/GN/GE are consistent with the cubic structure of free Fe_3O_4 nanostructures, implying that there is no structural change even after the composite preparation. In addition, there is a new diffraction peak at $2\theta \approx 25.77°$ in Fe_3O_4/GN and Fe_3O_4/GN/GE composite, which could be credited to the GN, ensuring the composite fabrication of Fe_3O_4 with GN sheets. Moreover, there is no change in the crystalline morphology of Fe_3O_4/GN and Fe_3O_4/GN/GE composite, enunciating that the GE layer does not change the crystalline morphology of Fe_3O_4/GN.

The components responsible for the capping on the prepared Fe_3O_4/GN/GE nanocomposite are analyzed by FTIR and the FTIR spectrums of Fe_3O_4 NPs, Fe_3O_4/GN, and Fe_3O_4/GN/GE nanocomposite and GE are shown in Fig. 3b. There is an intense peak at ~ 583 cm^{-1} in the spectrum of Fe_3O_4 NPs, Fe_3O_4/GN, and Fe_3O_4/GN/GE nanocomposite, as shown in Fig. 3b, corresponding to the Fe–O stretching vibration [38]. From GE, the characteristic adsorption peaks located at 524, 1023, 1121, 1270, 1632, 2937, and 3416 cm^{-1} identify the S–S, C–S, C=S, S–CH_2–, –NH, –CH_2–, and –CO–NH vibration of GE, respectively, which manifested that the components of GE include organic sulfide, sulfoether compounds, and acid amides. Furthermore, these entire characteristic peaks exit in the FTIR spectrum of Fe_3O_4/GN/GE, declaring the valid incorporation of GE in the Fe_3O_4/GN nanocomposite.

Table 1 Identity and chemical structures of compounds in garlic extract

Peak No.	Retention time (min)	Compound	Structure
1	1.78	Ethyl Acetate	
2	1.97	3-methyl-Butanal	
3	2.46	1,1-diethoxy-ethan homopolymer	
4	4.67	1,3-Dithiane	
5	4.69	Allyl methyl disulphide	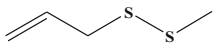
6	7.03	Diallyl disulphide	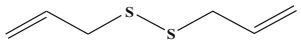
7	8.69	3-vinyl-1,2-dithiacyclohex-4-ene	
8	9.05	3-vinyl-1,2-dithiacyclohex-5-ene	
9	10.32	Diallyl trisulfide	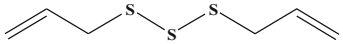

Electrochemical characterizations

The cyclic voltammetries (CVs) of different modified electrodes in 5.0 mmol/L $K_3[Fe(CN)_6]$ containing 0.1 mol/L KCl are shown in Fig. 4a, which have studied the change of electrode behavior of each modified electrodes. All of the electrodes exhibited two well-defined redox peaks of $[Fe(CN)_6]^{3-/4-}$. However, the redox peak currents of each electrode were different. The redox peak current of Fe_3O_4/GN/GCE was higher than the redox peak current of GCE, while the redox peak current of Fe_3O_4/GN/GE/GCE was lower than the redox peak current of Fe_3O_4/GN/GCE. This phenomenon can be ascribed to the Fe_3O_4/GN enabled fast electron transport through the underlying GN layer to Fe_3O_4 nanoparticles [35, 39] and the GE layer obstructed the electron transport, respectively (EIS see Supplementary information).

We have studied the electrochemical features and the function for Pb^{2+} analysis of the Fe_3O_4/GN/GE by comparing

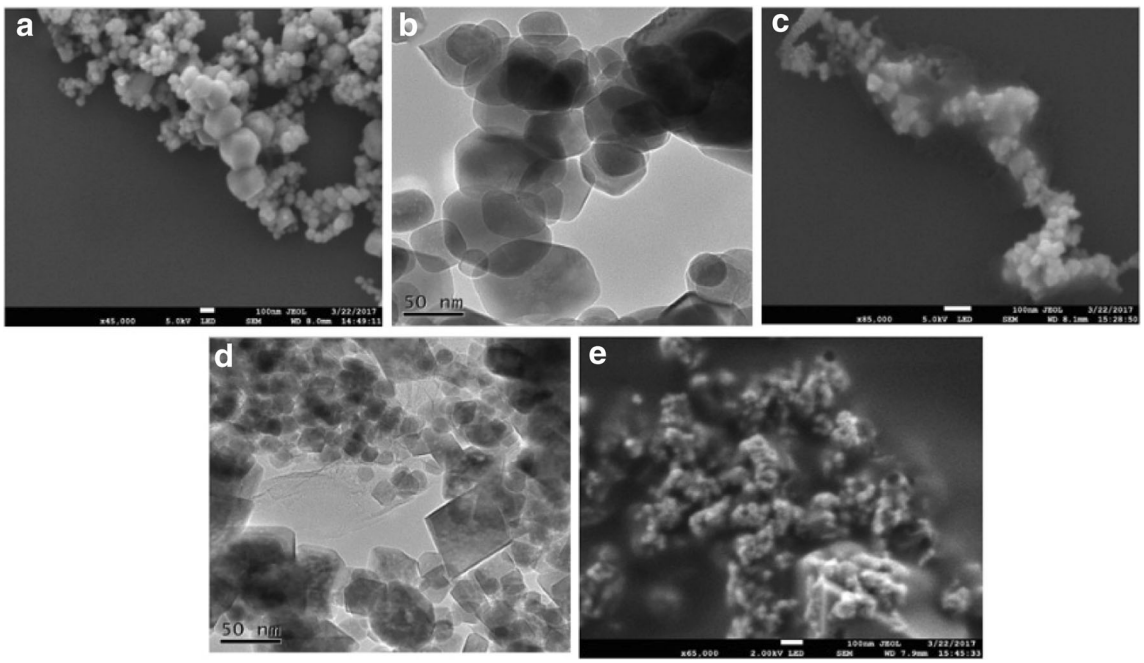

Fig. 2 SEM and TEM images of **a**, **b** Fe3O4 NPs and **c**, **d** Fe3O4/GN composite. SEM images of Fe3O4/GN/GE composite

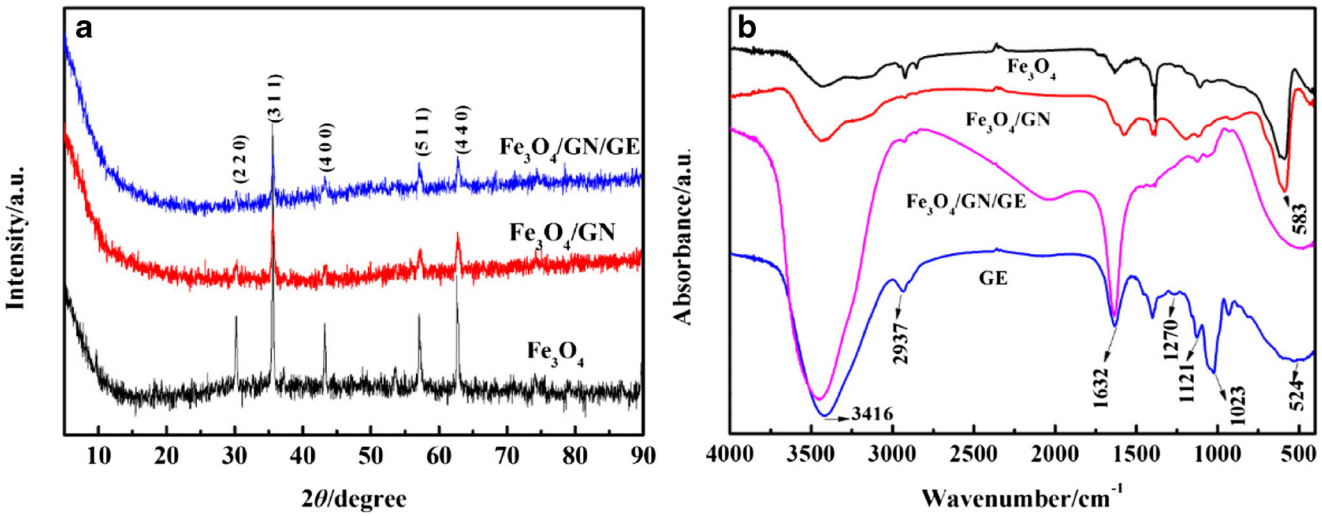

Fig. 3 **a** XRD patterns of Fe3O4 NPs, Fe3O4/GN, and Fe3O4/GN/GE. **b** FTIR spectra of Fe3O4 NPs, Fe3O4/GN, and Fe3O4/GN/GE

the electrochemical SWV responses on several modified electrodes in the presence of 1 μM target Pb^{2+} in pH 5.50 ABS, as seen in Fig. 5. After electrochemical accumulation at −1.0 V for 180 s, a well-defined stripping peak appears at the potential values between −0.55 and − 0.60 V with different stripping peak current on all electrodes. There is an inconspicuous stripping peak at −0.57 V on bare GCE, and its stripping peak current for Pb^{2+} is far less than that of other electrodes. The Fe_3O_4 and Fe_3O_4/GN have a larger surface area between the electrode and electrolyte solution. In contrast, the peak current sharply increased upon addition of GE on the Fe_3O_4/GN, which can form strong complex with Pb^{2+} and provide more active sites for Pb^{2+} accumulation. All of those results could certify that the interaction between target Pb^{2+} and Fe_3O_4/GN/GE has changed the electronic signal, thus providing a possibility for the recognition of Pb^{2+}.

Optimization of assay conditions

Various experimental parameters were optimized for exploiting the maximum efficacy of Fe_3O_4/GN/GE/GCE sensor with care, loading of Fe_3O_4/GN/GE, analyte accumulation time, and pH of buffer solution included. As portrayed in Fig. 6a, the effect of the coated Fe_3O_4/GN/GE composite on electrode was shown. The peak current increased with the volume of the coated Fe_3O_4/GN/GE composite on electrode, and then reached maximum when the volume of Fe_3O_4/GN/GE composite on electrode is 5 μL. Therefore, in the subsequent measurements, 5 μL Fe_3O_4/GN/GE composite are coated on electrode. As seen from Fig. 6b, the electrochemical signal of the developed biosensor enhanced rapidly as the analyte accumulation time increased and achieved a plateau at 180 s, which may be owing to the increase of composites film and decrease the electron transfer rate of metal stripping.

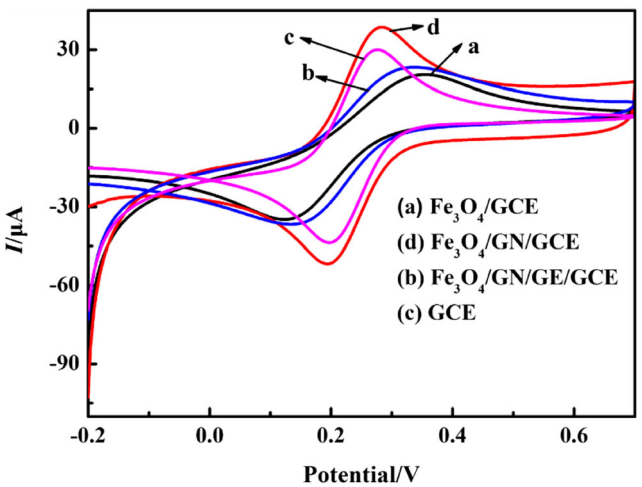

Fig. 4 Cyclic voltammograms for each immobilization step in 5.0 mmol/L K3[Fe(CN)6] containing 0.1 mol/L KCl solution

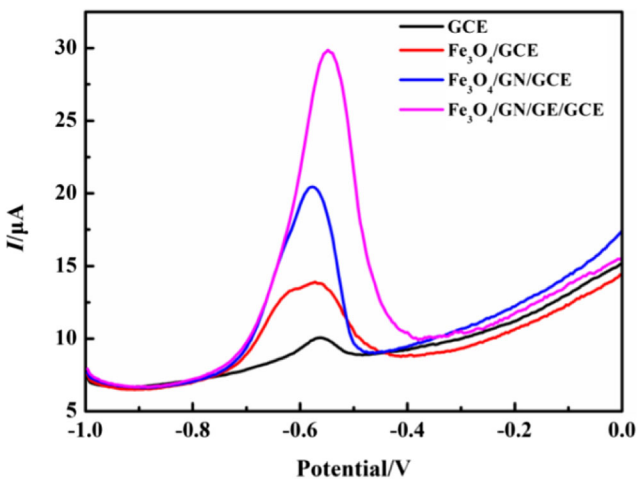

Fig. 5 SWVs recorded at Fe3O4/GCE, Fe3O4/GN/GCE, and Fe3O4/GN/GE/GCE in the presence of 1 μM Pb2+ in pH 5.50 ABS

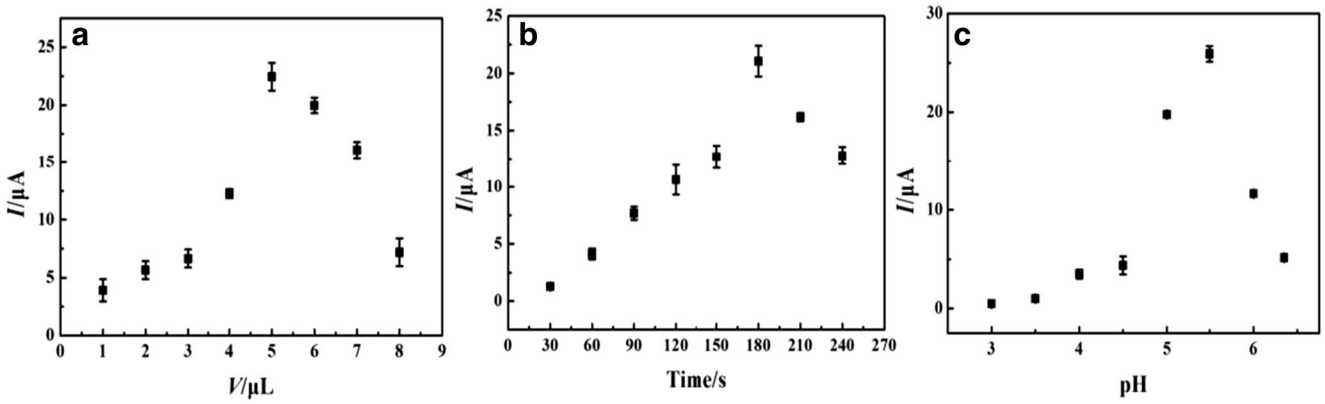

Fig. 6 Effects of **a** volume of coated composites on GCE, **b** accumulation time, and **c** pH value on the striping peak current. Error bars are the standard deviation for three consecutive measurements. Error bars are the standard deviation for three consecutive measurements

So, an analyte accumulation time of 180 s was employed as the optimum analyte accumulation time. The influence of the acidity of the electrolyte on the determination of Pb^{2+} in the range of 3.00~6.50 was optimized. As shown in Fig. 6c, it can be seen that the current value increased tardily with the pH of electrolyte in the range from 3.00 to 4.50, while the peak current enhanced rapidly with the pH of electrolyte in the range from 4.50 to 5.50 and obtained the maximum at 5.50. Thus, a pH of 5.50 was chosen as the optimized pH of electrolyte.

Analytical performance

Figure 7 depicts the SWV responses of the Fe_3O_4/GN/GE biosensor at different concentrations of Pb^{2+} under the optimal conditions. As portrayed in Fig. 7a, the SWV peaks increased with the increasing target Pb^{2+} concentrations and reached to plateau at concentration of 1000 nM Pb^{2+}. Furthermore, it is linear with the concentrations of Pb^{2+} from 0.001 to 0.5 nM and 0.5 to 1000 nM with correlation coefficients of 0.9999 and 0.9975, respectively (Fig. 7b). The linear regression equations were $y(\mu A) = 2.7262 + 23.0585x(nM)$ and $y(\mu A) = 14.2501 + 0.0102x(nM)$. The detection limit (LOD) and quantification limit (LOQ) of the biosensor were determined to be 0.0123 and 0.041 pM based on three times the standard deviation of the blank sample/slope and ten times the standard deviation of the blank sample/slope, respectively. The as-prepared biosensor based on novel Fe_3O_4/GN/GE showed favorable Pb^{2+} detection performances, compared with that of other Pb^{2+} biosensors in Table 2, highlighting its sensitivity and acceptability further. Our biosensor

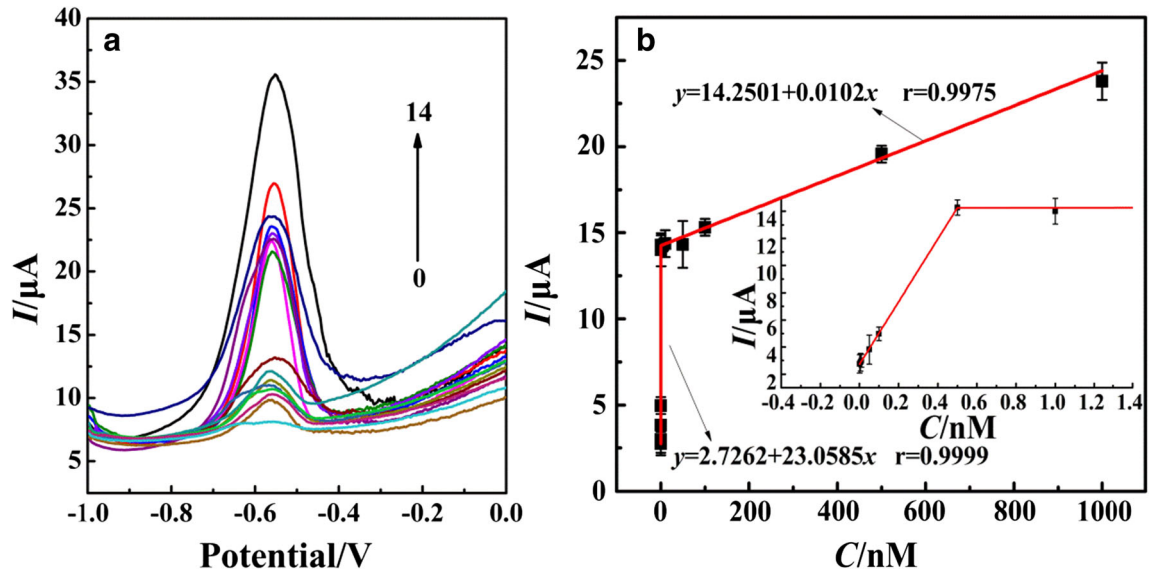

Fig. 7 **a** SWV curves of Fe3O4/GN/GE/GCE electrodes in 0.1 mol/L ABS (pH = 5.50) containing different concentrations of Pb2+ solution: 0, 0.001, 0.005, 0.01, 0.05, 0.1, 0.5, 1, 5, 10, 50, 100, 500, and 1000 nM. **b** Plot of the peak current against the concentration of Pb2+. Error bars are the standard deviation for three consecutive measurements

Table 2 Comparison of analytical properties of different modified electrode toward Pb^{2+}

Lead sensor	Methods	Sensitivity (μA/nM)	LDR (nM)	LOD (pM)	References
NPG/AQDS/GR–5DNAzyme/GCE	DPV	− 0.35839	1–120	20	[40]
Fc–ssDNAzyme/Au	DPV	–	0.5–5000	25	[41]
Au–Pd/hemin/Gquadruplex-based DNAzyme	DPV	0.07263	0.001–100	0.34	[42]
OMC–GNPs/DNAzyme	EIS	–	0.5–50,000	200	[43]
Au/FrGO/Au–PWE	DPV	−0.28233	0.005–2000	2	[44]
AuNPs-Apt-CS-modified	DPV	0.1498	0.6–50	312	[45]
5-Br-PADAP/MWCNT/GCEs	DPA	0.031	4.4–553.6	483	[46]
CPEa-CD and CPEb-CD	CV	0.00137 0.00305	10,000–1,000,000	–	[47]
Glassy carbon spheres	DPV	–	1000–10,000	180,000	[48]
PDMS-PA-DB18C6	DPASV	0.0039	96–3381.6	16,908	[49]
PMOs	SWASV	0.036	9.6–480	2415	[50]
Fe_3O_4/GN/GE/GCE	SWV	23.0585 0.0102	0.001–0.5 0.5–1000	0.0123	This work

NPG nanoporous gold, *AQDS* disodium–anthraquinone–2, 6–disulfonate, *Fc* redox–active ferrocene, *OMC–GNPs* ordered mesoporous carbon–gold nanoparticle, *Apt* aptamer, *CS* complementary strand, *CD* cyclodextrins, *PDMS-PA-DB18C6* A siloxane-crown ether polyamide copolymer, *PMOs* periodic mesoporous organosilica

provides an attractive detection limit and a broader working range. Besides, the developed biosensor has advantages in fabrication with a facile hydrothermal technique without any surfactants or templates, economy without the use of DNAzyme and with the utilization of the natural substance GE for Pb^{2+} ion-specific, and environmentally friendly without any toxicant and with the employ of the environmental benignity Fe_3O_4/GN/GE composite. All of these comparison manifest that the sensing performance of the designed method is superior to the mentioned biosensor for Pb^{2+} determination.

Reproducibility and stability of the proposed sensor

The reproducibility and stability are the extremely important features of the biosensor in its practical applications and development. In our work, the reproducibility of the as-proposed Pb^{2+} biosensor was evaluated by estimating the variation of the SWV response to 1000 nM Pb^{2+} for eight different Fe_3O_4/GN/GE electrodes. According to the experimental results, as shown in Fig. 8a, the SWV response variation of the assays with the same-batch biosensors is 3.61%, revealing the good reproducibility of this method. Additionally, the stability of the as-prepared biosensor was also explored on a 10-week period. The biosensor was stored in the refrigerator (4 °C) when not in use and measured intermittently (per 7 days). The SWV response remained stable (RSD 6.28%) and preserved 86.14% of the initial response after a storage period of 10 weeks for the recognition of 1000 nM Pb^{2+}, as portrayed in Fig. 8b. All of these results indicated that the reproducibility and stability of the developed biosensor were desirable.

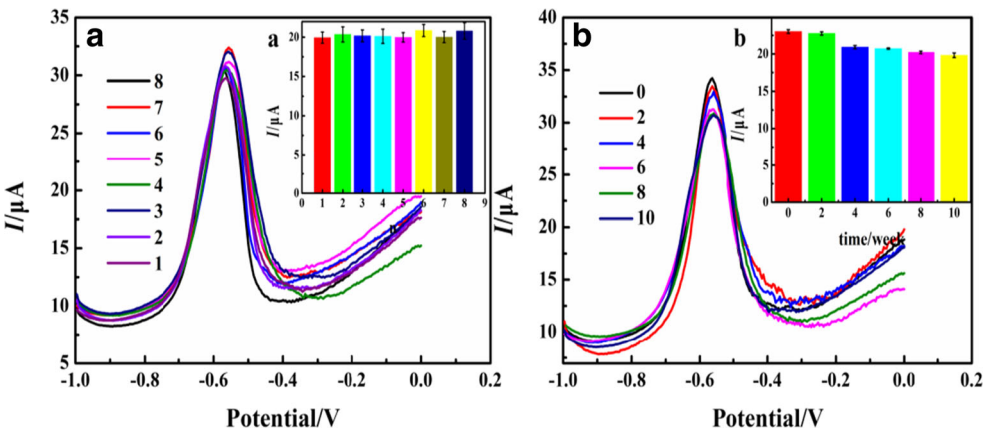

Fig. 8 **a** SWV curves of eight different Fe3O4/GN/GE/GCE in 0.1 mol/L ABS (pH = 5.50) containing 1000 nM Pb2+. Inset (a) is the reproducibility of the eight different modified electrodes by SWV. **b** SWV curves of the different preserved time Fe3O4/GN/GE/GCE in 0.1 mol/L ABS (pH = 5.50) containing 1000 nM Pb2+. Inset (b) is the stability of the proposed sensor. Error bars are the standard deviation for three consecutive measurements

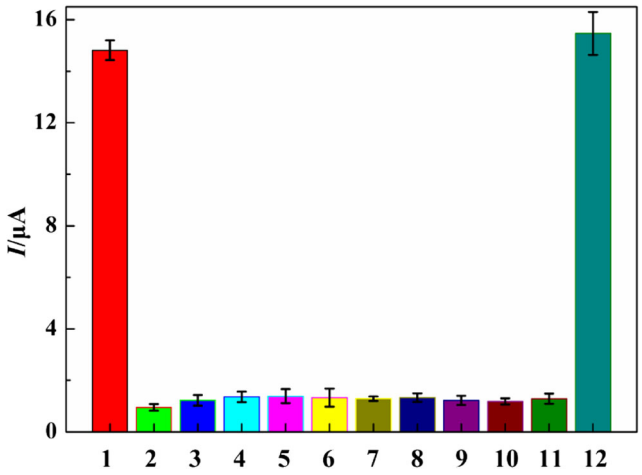

Fig. 9 The selectivity of the proposed sensor. The interfering cations are listed in order (1 to 12): (1) Pb2+, (2) blank, (3) Co2+, (4) Fe3+, (5) Cu2+, (6) Mn2+, (7) Zn2+, (8) Ni2+, (9) Ag+, (10) Hg2+, (11) Cd2+, and (12) all the interference mix with 0.5 nM Pb(II)

Specificity of the proposed sensor

The specificity of the designed strategy is supposed to be validated to ensure that the biosensor was acceptable before it was applied to the real sample analysis. We challenged the system against other ions including Co^{2+}, Fe^{3+}, Cu^{2+}, Mn^{2+}, Zn^{2+}, Ni^{2+}, Ag^{+}, Hg^{2+}, and Cd^{2+} to investigate the specificity of our designed strategy. Figure 9 depicts the histograms of peak current changes for the biosensor after reaction with other interfering metal ions. Obviously, the current response was much higher with the target Pb^{2+} of 0.5 nM than those of other interfering metal ions (10 nM). The results clearly demonstrated that the sensing strategy could monitor Pb^{2+} in the presence of other metal ions selectively.

Application for the analysis of samples

We have determined Pb^{2+} in real samples (tap water, rain water, and river water from Jialing River located in Chongqing, China) by measuring the recovery of Pb^{2+} to evaluate the utility of the fabricated biosensor. To get rid of insoluble substance, all samples were filtered by a filter membrane before detected. We have summarized the recovery values of the real samples, as shown in Table 3. All recovery values range from 91.7 to 99.8% and RSD were 2.33~5.7%, which verify that the developed sensing strategy was potentially applicable for practical detection in real samples.

Conclusions

In this study, we have fabricated a novel cheap and sensitive electrochemical sensor using Fe_3O_4/GN composite and GE as electrode modification materials for Pb^{2+} determination. It is first reported that natural substance garlic extract was utilized as Pb^{2+} specific-receptor and modified with Fe_3O_4-graphene composite for establishing advanced sensing devices. The novel sensor not only showed high sensitivity and selectivity for Pb^{2+} but also exhibited broad linearity, low detection limit, and satisfactory reproducibility and stability. Additionally, the practical application in detecting real water samples shows a satisfactory result. In general, this novel sensor possesses superior electrochemical detection performance and less cost compared with other published electrochemical sensor.

Table 3 Determination of Pb(II) recovery by the suggested sensor in different water samples (nmol/L)

Samples	Pb^{2+} added	Pb^{2+} found[a]	Recovery (%)	RSD (%)
Tap water	0	0.0263 (±0.0011)		3.23
	0.1	0.118 (±0.031)	91.7 ± 0.6	5.7
	1000	956 (±7.34)	95.6 ± 0.3	3.04
	0	0.0996(±0.0012)		2.33
Rain water	0.1	0.0197(±0.0036)	97.4 ± 0.5	5.01
	1000	975(±11.97)	97.5 ± 0.49	4.95
	0	0.177(±0.021)		3.15
River water	0.1	0.274(±0.03)	97.1 ± 0.33	3.28
	1000	999(±13.7)	99.8 ± 0.56	5.61
	0	0.253(±0.043)		2.64
Industrial effluents	0.1	0.356(±0.057)	103.9 ± 0.57	3.86
	1000	1003(±12.36)	100.3 ± 0.52	4.92

[a] Average of three replicate measurements

Funding This work was supported by the National Natural Science Foundation of China (No. 31101284), the Graduate Research and Innovation Foundation of Chongqing, China (No. CYS17017), Chongqing Science and Technology Commission (No. CSTC2015shmszxl20097 and CSTC2017shmsA100010), the Fundamental Research Funds for the Central Universities (No. 2018CDXYHG0028), and the Chongqing University Student Research Training Program (No. CQU-SRTP-2016330 and CQU-SRTP-2016337).

References

1. Aposhian HV, Maiorino RM, Ramirez DG, Charles MZ, Xu Z, Hurlbut KM, Munoz PJ, Dart RC, aposhian MM (1995) Mobilization of heavy metals by newer, therapeutically useful chelating agents. Toxicology 97(1-3):23–38
2. Kim JM, Ghang N, Kim WK, Chun HS (2006) Dietary S-allyl-L-cysteine reduces mortality with decreased incidence of stroke and behavioral changes in stroke-prone spontaneously hypertensive rats. Biosci Biotechnol Biochem 70(8):1969–1971
3. Lee YJ, Lee D, Shin SM, Lee JS, Chun HS, Quan FS, Shin JH, Lee GJ (2017) Potential protective effects of fermented garlic extract on myocardial ischemia-reperfusion injury utilizing in vitro and ex vivo models. J Funct Foods 33:278–285
4. Calle MM, Capote FP, Luque de Castro MD (2017) Headspace −GC–MS volatile profile of black garlic vs fresh garlic: evolution along fermentation and behavior under heating. LWT-Food Sci Technol 80:98–105
5. Tocmo R, Wu Y, Liang D, Fogliano V, Huang D (2017) Boiling enriches the linear polysulfides and the hydrogen sulfide-releasing activity of garlic. Food Chem 221:1867–1873
6. Piątkowska E, Kopeć A, Leszczyńska T (2015) Basic chemical composition, content of micro- and macroelements and antio xidant activity of different varieties of garlic's leaves Polish origin. ŻYWNOŚĆ. Nauka. Technologia. Jakość 1:181–192
7. Szychowski KA, Binduga UE, Rybczyńska-Tkaczyk K, Leja ML, Gmiński J (2016) Cytotoxic effects of two extracts from garlic (*Allium sativum* L.) cultivars on the human squamous carcinoma cell line SCC-15. Saudi J Biol Sci. doi: https://doi.org/10.1016/j.sjbs.2016.10.005
8. Lanzotti V (2006) The analysis of onion and garlic. J Chromatogr A 1112(1-2):3–22
9. Bhandari PR (2012) Garlic (*Allium sativum* L.): a review of potential therapeutic application. International Journal of Green Pharmacy (Medknow Publications 6: 118
10. Fatima RA, Ahmad M (2006) Certain antioxidant enzymes of Allium cepa as biomarkers for the detection of toxic heavy metals in wastewater. Sci Total Environ 346:256–273
11. Cheng Y, Fa H, Yin W, Hou C, Huo D, Liu F (2015) A sensitive electrochemical sensor for lead based on gold nanoparticles/nitrogen-doped graphene composites functionalized with l-cysteine-modified electrode. J Solid State Electr 20:327–335
12. Zhou W, Li C, Sun C, Yang Y (2016) Simultaneously determination of trace Cd^{2+} and Pb^{2+} based on L-cysteine/graphene modified glassy carbon electrode. Food Chem 192:351–357
13. Abnous K, Danesh NM, Alibolandi M, Ramezani M, Sarreshtehdar EA, Zolfaghari R, Seyed MT (2017) A new amplified π-shape electrochemical aptasensor for ultrasensitive detection of aflatoxin B_1. Biosens Bioelectron 94:374–379
14. Su J, Cao M, Ren L, Hu C (2011) Fe_3O_4–graphene nanocomposites with improved lithium storage and magnetism properties. J Phys Chem C 115(30):14469–14477
15. Boruah PK, Sharma B, Hussain N, Das MR (2017) Magnetically recoverable Fe_3O_4/graphene nanocomposite towards efficient removal of triazine pesticides from aqueous solution: investigation of the adsorption phenomenon and specific ion effect. Chemosphere 168:1058–1067
16. Wang B, Park J, Wang C, Ahn H, Wang G (2010) Mn_3O_4 nanoparticles embedded into graphene nanosheets: preparation, characterization, and electrochemical properties for supercapacitors. Electrochim Acta 55:6812–6817
17. Chandra V, Park J, Chun Y, Lee JW, Hwang I, Kim KS (2010) Water-dispersible magnetite-reduced graphene oxide composites for arsenic removal. ACS Nano 4(7):3979–3986
18. Pumera M (2010) Graphene-based nanomaterials and their electrochemistry. Chem Soc Rev 39(11):4146–4157
19. He Y, Sheng Q, Zheng J, Wang M, Liu B (2011) Magnetite–graphene for the direct electrochemistry of hemoglobin and its biosensing application. Electrochim Acta 56(5):2471–2476
20. Gao Y, Ma D, Hu G, Zhai P, Bao X, Zhu B, Zhang B, Su DS (2011) Layered-carbon-stabilized iron oxide nanostructures as oxidation catalysts. Angew Chem 50(43):10236–10240
21. Hsieh CT, Lin JY, Mo CY (2011) Improved storage capacity and rate capability of Fe_3O_4–graphene anodes for lithium-ion batteries. Electrochim Acta 58:119–124
22. Zhuo L, Wu Y, Wang L, Ming J, Yu Y, Zhang X, Zhao F (2013) CO_2–expanded ethanol chemical synthesis of a Fe_3O_4@graphene composite and its good electrochemical properties as anode material for Li-ion batteries. J Mater Chem A 1(12):3954–3960
23. He J, Zhao S, Lian Y, Zhou YM, Wang L, Ding B, Cui S (2017) Graphene-doped carbon/Fe_3O_4 porous nanofibers with hierarchical band construction as high-performance anodes for lithium-ion batteries. Electrochim Acta 229:306–315
24. Wang D, Li Y, Wang Q, Wang T (2012) Nanostructured Fe_2O_3–graphene composite as a novel electrode material for supercapacitors. J Solid State Electr 16(6):2095–2102
25. Wu B, Ren Y, Mu D, Liu X, Zhao J, Wu F (2013) Enhanced electrochemical performance of LiFePO cathode with the addition of fluoroethylene carbonate in electrolyte. J Solid State Electr 17(3):811–816
26. Zhang W, Wang L, Zheng X (2014) Indicator-free electrochemical genosensing originated from the self-signal of poly-xanthurenic acid enhanced by Fe_3O_4/reduced graphene oxide. J Solid State Electr 18(9):2367–2373
27. Liu HD, Zhang JL, Xu DD, Huang LH, Tan SZ, Mai WJ (2015) Easy one-step hydrothermal synthesis of nitrogen-doped reduced graphene oxide/iron oxide hybrid as efficient supercapacitor material. J Solid State Electr 19(1):135–144
28. Suryawanshi A, Aravindan V, Mhamane D, Yadav P, Patil S, Madhavi S, Ogale S (2015) Excellent performance of Fe_3O_4-perforated graphene composite as promising anode in practical Li-ion configuration with $LiMn_2O_4$. Energy Storage Materials 9:152–157
29. Zhou G, Wang D, Li F, Zhang L, Li N, Wu Z, Wen L, Lu GQ (Max), Cheng H (2010) Graphene-wrapped Fe_3O_4 anode material with improved reversible capacity and cyclic stability for lithium ion batteries. Chem Mater 22: 5306–5313, 18
30. Liang CL, Liu Y, Bao RY, Luo Y, Yang W, Xie BH, Yang MB (2016) Effects of Fe_3O_4 loading on the cycling performance of Fe_3O_4/rGO composite anode material for lithium ion batteries. J Alloy Compd 678:80–86
31. Buica GO, Lazar IG, Saint AE, Tecuceanu V, Dumitriu C, Anton IA, Stoian AB, Ungureanu EM (2017) Ultrasensitive modified electrode based on poly(1*H* -pyrrole-1-hexanoic acid) for Pb(II) detection. Sens Actuat B: Chem 246:434–443
32. Qin D, Gao S, Wang L, Shen H, Yalikun N, Sukhrobov P, Wagberg T, Zhao Y, Mamat X, Hu G (2017) Three-dimensional carbon nanofiber derived from bacterial cellulose for use in a Nafion matrix on a glassy carbon electrode for simultaneous voltammetric determination of trace levels of Cd(II) and Pb(II). Microchim Acta 184(8):2759–2766

33. Pérez-Ràfols C, Bastos-Arrieta J, Serrano N, Díaz-Cruz JM, Ariño C, Pablo JD, Esteban M (2017) Ag nanoparticles drop-casting modification of screen-printed electrodes for the simultaneous voltammetric determination of Cu(II) and Pb(II). Sensors-Basel 17(6):1458–1469
34. Dönmez KB, Çetinkaya E, Deveci S, Karadağ S, Şahin Y, Doğu M (2017) Preparation of electrochemically treated nanoporous pencil-graphite electrodes for the simultaneous determination of Pb and Cd in water samples. Ana bioanal Chem 409(20):4827–4837
35. Wang Q, Jiao L, Du H, Wang Y, Yuan H (2014) Fe_3O_4 nanoparticles grown on graphene as advanced electrode materials for supercapacitors. J Power Sources 245:101–106
36. Li L, Gao P, Gai S, He F, Chen Y, Zhang M, Yang P (2016) Ultra small and highly dispersed Fe_3O_4 nanoparticles anchored on reduced graphene for supercapacitor application. Electrochim Acta 190:566–573
37. Atarod M, Nasrollahzadeh M, Sajadi SM (2015) Green synthesis of a Cu/reduced graphene oxide/Fe_3O_4 nanocomposite using *Euphorbia wallichii* leaf extract and its application as a recyclable and heterogeneous catalyst for the reduction of 4-nitrophenol and rhodamine B. RSC Adv 5(111):91532–91543
38. Rani GJ, Babu KJ, kumar GG, Rajan MAJ (2016) *Watsonia meriana* flower like Fe_3O_4/reduced graphene oxide nanocomposite for the highly sensitive and selective electrochemical sensing of dopamine. J Alloy Compd 688:500–512
39. Shi W, Zhu J, Sim DH, Tay YY, Lu Z, Sharma Y, Srinivasan M, Zhang H, Hng Huey H, Yan Q (2011) Achieving high specific charge capacitances in Fe_3O_4/reduced graphene oxide nanocomposites. J Mater Chem 21(10):3422–3427
40. Zhou Y, Zhang J, Tang L, Peng B, Zeng G, Luo L, Gao J, Pang Y, Deng Y, Zhang F (2017) A label-free GR-5DNAzyme sensor for lead ions detection based on nanoporous gold and anionic intercalator. Talanta 165:274–281
41. Zhang Y, Xiao S, Li H, Liu H, Pang P, Wang H, Wu Z, Yang W (2016) A Pb^{2+}-ion electrochemical biosensor based on single-stranded DNAzyme catalytic beacon. Sens Actuat B: Chem 222: 1083–1089
42. Zhou Q, Lin Y, Lin Y, Wei Q, Chen G, Tang D (2016) Highly sensitive electrochemical sensing platform for lead ion based on synergetic catalysis of DNAzyme and Au-Pd porous bimetallic nanostructures. Biosens Bioelectron 78:236–243
43. Zhou Y, Tang L, Zeng G, Zhang C, Xie X, Liu Y, Wang J, Tang J, Zhang Y, Deng Y (2016) Label free detection of lead using impedimetric sensor based on ordered mesoporous carbon-gold nanoparticles and DNAzyme catalytic beacons. Talanta 146:641–647
44. Ge S, Wu K, Zhang Y, Yan M, Yu J (2016) Paper-based biosensor relying on flower-like reduced graphene guided enzymatically deposition of polyaniline for Pb^{2+} detection. Biosens Bioelectron 80: 215–221
45. Taghdisi SM, Danesh NM, Lavaee P, Ramezani M, Abnous K (2016) An electrochemical aptasensor based on gold nanoparticles, thionine and hairpin structure of complementary strand of aptamer for ultrasensitive detection of lead. Sens Actuat B: Chem 234:462–469
46. Morales GR, Silva TR, Galicia L (2003) Carbon paste electrodes electrochemically modified with cyclodextrins. J Solid State Electr 7(6):355–360
47. Salmanipour A, Taher MA (2011) An electrochemical sensor for stripping analysis of Pb(II) based on multiwalled carbon nanotube functionalized with 5-Br-PADAP. J Solid State Electr 15(11–12): 2695–2702
48. Raghu GK, Sampath S, Pandurangappa M (2012) Chemically functionalized glassy carbon spheres: a new covalent bulk modified composite electrode for the simultaneous determination of lead and cadmium. J Solid State Electr 16(5):1953–1963
49. Simionca IM, Arvinte A, Ardeleanu R, Pinteala M (2012) Siloxane-crown ether polyamide based electrode for electrochemical determination of lead(II) in aqueous solution. Electroanal 24(10):1995–2004
50. Morante-Zarcero S, Pérez-Quintanilla D, Sierra I (2015) A disposable electrochemical sensor based on bifunctional periodic mesoporous organosilica for the determination of lead in drinking waters. J Solid State Electr 19(7):2117–2127